Detailed Characterization of Optical Fibers by Combining S^2 Imaging With Correlation Filter Mode Analysis

Clémence Jollivet, Daniel Flamm, Michael Duparré, and Axel Schülzgen

***Abstract*—Spatially and spectrally resolved imaging (S^2 imaging) and correlation filter technique (CFT) are two very different, widespread fiber mode analysis techniques. Both techniques have been successfully employed to decompose few-modes and multi-mode beams respectively. In this study, we present a novel experimental tool combining S^2 imaging and CFT mode analyses in a unique system. We demonstrate that both methods are complementary with the ability to fully resolve scalar and vector-valued transverse modal fields. Using results from the combined experiment, mode powers (ρ^2) evaluated from CFT analysis and S^2 imaging are directly compared for a wide range of fiber beams (from single- to multi-mode). As a result, we experimentally identify the mode detection limit of each mode analysis and prove that S^2 imaging accuracy range can be considerably increased employing an analytical mode evaluation method. The conclusion contains a table summarizing the expertise of each mode analysis.**

***Index Terms*—Fiber characterization, fiber optics, large-mode area fiber.**

I. Introduction

RECENT developments in optical fibers have successfully enabled average and peak power scaling of fiber-based amplifier and laser systems [1], [2]. In particular, large mode area (LMA) fibers, supporting large core sizes ($\geq$20 μm in diameter) to scale surface damage limitation of fused silica and to reduce non-linearities, seem to be very good candidates according to recent output performances [3], [4]. An intrinsic challenge when designing LMA fibers is to engineer low numerical aperture ($\leq$0.07) to limit the number of guided higher order modes (HOMs). HOMs carrying a significant fraction of light can strongly affect the output beam profile, degrading the beam M^2 parameter which is detrimental for most high power applications requiring diffraction limited beam quality with $M^2 \sim 1$ [5]–[7]. In addition, further output power scaling of LMA-fiber lasers and amplifiers is recently limited by the onset of mode-instabilities caused by the formation of thermal gratings [8]. On the other hand, it has also been demonstrated that measured good beam quality ($M^2 \sim 1$) does not ensure single-mode propagation [9].

In a context where modal instabilities seem to be the main limitation to power scaling in fiber–based lasers and where the diversity of novel specialty LMA fiber designs offering diffraction-limited beam quality is increasing, there is an important need for complete and accurate mode analysis tools. Up to this date, several mode analysis techniques have been demonstrated. Among the most employed one, we can refer to spatially and spectrally resolved imaging (S^2 imaging) [10], low coherence interferometry [11], correlation filter technique (CFT) [12], cross-correlated imaging [13] and high-speed modal decomposition [14]. One technique is preferred according to the type of beam to be decomposed (single-mode (SM) or multi-mode (MM)) and depending on the modal information to access.

In this paper, we combine two very different mode analysis techniques recently demonstrated and successfully implemented, namely S^2 imaging and CFT analysis, in a unique novel experimental tool. After motivating our study with a comprehensive review of each mode analysis in Section II, the combined experiment is detailed in Section III. In Section IV, we introduce the unique capability offered by the combined experiment in performing an advanced modal characterization of optical fibers. Finally, in Section V, a large variety of beams (from SM to MM) are decomposed with the combined experiment. Individual mode powers (ρ^2) are evaluated with S^2 imaging and CFT and are directly compared, leading to a discussion on the mode detection limit of each technique.

II. Review of S^2 Imaging and CFT Mode Analyses

The recent and large success of S^2 imaging and CFT analysis is noteworthy. This section briefly introduces each technique and lists their most recent applications. The considerable impact of these techniques on the development of fiber technologies and fiber systems is emphasized.

A. S^2 Imaging Mode Analysis

The first tecshnique, S^2 imaging, also called spatially and spectrally resolved imaging, has been introduced for the first time by Nicholson *et al.* [10]. In optical fibers, each guided modes propagates at a different speed (propagation constant) and spectrally interfere. The interference period of the so-called multimode-interference (MMI) pattern is fixed by the

Manuscript received July 19, 2013; revised November 14, 2013 and December 17, 2013; accepted December 23, 2013. Date of publication January 15, 2014; date of current version January 24, 2014. This work was supported by the Air Force Office of Scientific Research under Grant W911NF-10-1-0441.

C. Jollivet and A. Schülzgen are with the CREOL, College of Optics and Photonics, University of Central Florida, Orlando, FL 32816 USA (e-mail: jollivet@creol.ucf.edu; axel@creol.ucf.edu).

D. Flamm and M. Duparré are with the Institute of Applied Optics, Abbe Center of Photonics, Friedrich Schiller University Jena, Jena 07743, Germany (e-mail: daniel.flamm@uni-jena.de; michael.duparre@uni-jena.de).

Color versions of one or more of the figures in this paper are available online at http://ieeexplore.ieee.org.

Digital Object Identifier 10.1109/JLT.2013.2297337

differential group delay (DGD) between the two interfering modes. The principle of S^2 imaging is to measure the MMI pattern at several locations across the delivered beam using a scanning fiber probe. A Fourier analysis of the recorded spectra enables to resolve the DGD between two interfering modes and to reconstruct the corresponding amplitude and phase profiles. To date, this technique has offered an unmatched ability to accurately resolve strongly attenuated HOMs ($\sim$40 dB) with respect to the fundamental mode.

Recent applications include mode analysis of LMA fibers [10], [15], photonic crystal fibers [16], all-solid and hollow core band-gap fibers [17], [18], as well as extended long tapers [19] and 2 μm wide silicone waveguides [20]. S^2 imaging has also been successfully employed to measure HOM bend-loss in photonic band-gap fibers [21], to characterize efficient HOM suppression in scalable output fiber amplifiers [22], to prove increased performances of Q-switched 2 μm fiber lasers [23] and to study the impact of fiber boundaries on leaky modes [24]. To address an increasing demand for an S^2 imaging detection device, a commercial product been recently released using a tunable laser and a CCD to optimize the cost and the measurement time [25].

B. Correlation Filter Technique (CFT) Mode Analysis

The second mode analysis technique, originally introduced by Golub *et al.* [26], the so-called correlation filter technique, makes use of a matched computer-generated hologram (CGH). The CGH is fabricated according to the field distributions of guided modes in a fiber at a specific wavelength, numerically calculated using a mode solver [27]. The holographic filter is implemented into a simple Fourier setup to optically calculate the overlap integrals of the fiber near- field with the calculated modal transmission functions implemented on the filter. The far-field pattern diffracted by the CGH contains direct information regarding transverse mode powers and intermodal phase differences. It is particularly suitable for real time decomposition of MM fiber beams.

This technique has been employed to perform complete modal decomposition in amplitude, phase and polarization of LMA fibers [28] and multicore fibers [29]. Recently, spatial light modulators have been introduced as correlation filters, resulting in successful modal decompositions with the benefit of real-time switching of the digital hologram [30]. The CFT performances have been highlighted through a number of diverse applications such as measuring modally resolved bend-losses in few-modes fibers [31] and characterizing beams with orbital angular momentum [32]. Additional applications have recently emerged including fast M^2 measurement [33], wavefront reconstruction [34], mode division multiplexing and de-multiplexing [35], [36] and characterization of fiber-to-fiber coupling [37].

III. Combined Experiment

The experiment combining S^2 imaging and CFT is schematically represented in Fig. 1. A 60 nm broadband superluminescent diode (SLD) and a narrow linewidth laser, both fiber-coupled and emitting around 1064 nm wavelength, are used as

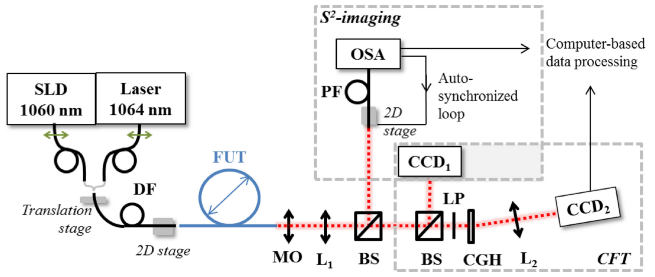

Fig. 1. Experiment combining S^2 imaging and CFT mode analysis. DF-delivery fiber, FUT-fiber under test, MO-microscope objective, L1-focusing lens, BS-non-polarizing 50/50 beam splitter, LP-linear polarizer, CGH-computer generated hologram, L2-lens, PF-probe fiber and OSA-optical spectrum analyzer.

light sources. The emitted light is coupled in a delivery fiber (DF) with a cut-off wavelength at 780 nm, ensuring SM propagation of the 1064 nm wavelength light. The input facet of a second piece of DF is mounted on a translation stage enabling to easily switch between light sources by changing the DF-to-DF alignment. The horizontal state of polarization of the incident light is maintained during propagation by coiling the fibers on an evenly flat horizontal surface.

The source is then coupled into the fiber under test (FUT) via the DF using a two-dimension translation stage. The near-field of the FUT is imaged using a microscope objective (MO) aligned in a 4-f configuration with a lens (L_1). Two 50/50 beam splitters (BS) split and direct the beam on CCD_1 for real-time measurement of the FUT near-field, on the probe fiber (PF) used for S^2 imaging mode analysis and on the CGH to perform CFT beam decomposition. CCD_1 is the common detector between S^2 imaging and CFT and serves as near-field measurement reference.

S^2 imaging is performed using the SLD light source. The PF stands on a two-dimensional motorized stage and is connected to an optical spectrum analyzer (OSA). The stage motion and the OSA are computer-synchronized for efficient time management while ensuring good spectral and spatial resolution.

Real-time CFT analysis is performed using the narrow-line laser source. The same FUT near-field as the one measured with S^2 imaging and CCD_1 is incident on a linear polarizer (LP) and is diffracted by the CGH, specifically designed and fabricated to resolve the modes guided by the FUT. The first diffraction order is imaged using a Fourier lens (L_2) on CCD_2 and the recorded intensity pattern is used for the identification of guided modes. More details are provided in Section IV.

The combined experiment presented in Fig. 1 allows performing both S^2 imaging and CFT to decompose one FUT beam. This can be achieved by proper alignment of the employed light source via the DF-to-DF coupling while maintaining the DT-to-FUT alignment fixed.

IV. Advanced Characterization of Optical Fibers

The FUT used in this experiment is a step-index LMA fiber commercialized by Fibercore with a core diameter of 20 μm and 0.07 NA. The resulting V-parameter at 1064 nm wavelength is

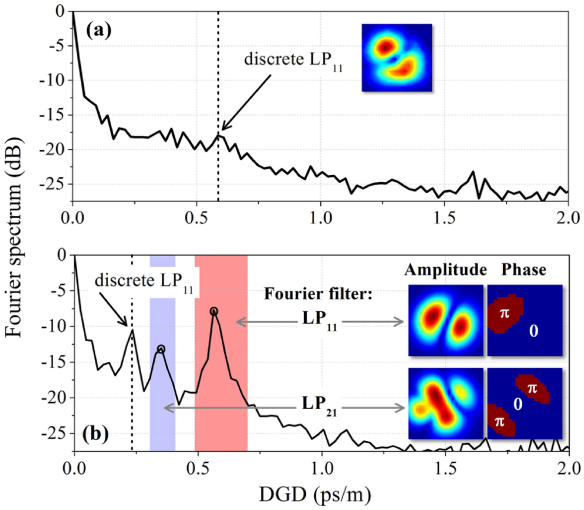

Fig. 2. Fourier spectrum calculated from S^2 imaging of a quasi-SM beam (a) and a MM beam (b). Discrete mode features are highlighted as well as Fourier filtering. In (b), the amplitude and phase profiles have been reconstructed at the DGD indicated by the black dots (0.35 ps/m and 0.56 ps/m).

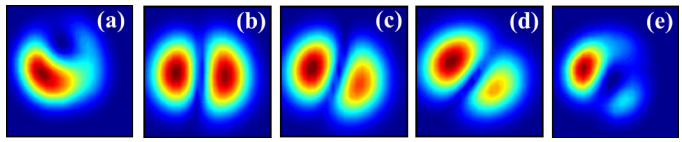

Fig. 3. (a)–(e): Modal amplitudes reconstructed at selected DGD within the Fourier filter highlighted in red in Fig. 2(b) (red area from 0.54 to 0.63 ps/m).

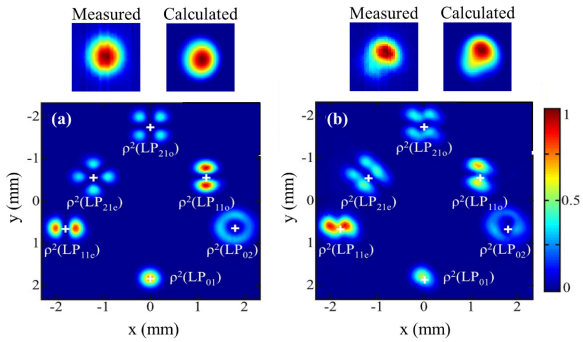

Fig. 4. Diffraction patterns measured on CCD_2 of the quasi-SM (a) and MM (b) beams. White crosses indicate the location of correlation answer for each mode of the FUT. The top inset displays the calculated vector-values FUT near-field compared to the measurement on CCD_1.

4.1, corresponding to a total of six guided LP modes: LP_{01}, $LP_{11e,o}$, $LP_{21e,o}$ and LP_{02}. However, the mode LP_{02} is guided too close to the cut-off to be measured. In this section, we introduce the procedure employed to analyze FUT beams measured with the combined experiment. The steps are illustrated using two examples: a quasi-SM beam and a MM beam. Various combinations of modes can be excited in the FUT (called FUT beams) by changing the mode overlap i.e. the DF-to-FUT coupling alignment. In the meantime, the FUT near-field is recorded on CCD_1 and the mode content is measured in real-time with CFT indicating the MM character of the FUT beam. Quasi-SM operation is obtained after perfect alignment of the DF with the FUT using additional coiling of the FUT (indicated by the blue arrow in Fig. 1) to further reduce remaining HOMs. Once a specific FUT beam is selected, the DF-to-FUT coupling conditions and coiling diameter are fixed.

The combined experiment is initiated by a first CFT analysis. Then, S^2 imaging is performed on the same FUT beam, followed by a second CFT measurement. Exact match between the two CFT measurements ensures a very stable FUT beam over the measurement time indicating a valid combined measurement.

The Fourier analyses of the measured S^2 imaging on the quasi-SM and MM beams are plotted in Fig. 2(a) and (b) respectively and follow the standard data analysis procedure [10].

The identification of temporal maxima in the Fourier spectrum arising from discrete and distributed mode scattering [15] provides information regarding modal amplitudes and phases. The peak at zero DGD, called DC component, contains the contribution from each excited mode propagating in the FUT. In Fig. 2(a), a single maximum at DGD $= 0.56$ ps/m is recorded from LP_{11} interfering with LP_{01} according to the reconstructed modal amplitude shown in inset. In comparison, the Fourier spectrum of the MM beam plotted in Fig. 2(b) exhibits several maxima. The modal amplitude and phase profiles have been reconstructed at two selected DGD showing evidence of guided LP_{11} and LP_{21} modes. As demonstrated by Jasapara *et al.* [25], discrete scattering in the Fourier spectrum can experience some broadening as the relative intermodal dispersion slightly changes across the measurement bandwidth (red and blue areas in Fig. 2(b)). Fig. 3 shows some reconstructed HOM amplitudes across the red highlighted region [see Fig. 2(b)].

As a result, after appropriate Fourier filtering, modal contributions from discrete scattering as well as broadened Fourier maxima are considered when evaluating the mode power of guided HOMs (see Section V).

The CFT section of the combined experiment completes the scalar modal field analysis from S^2 imaging. The diffraction patterns of the identical quasi-SM and MM beams have been recorded with CCD_2 and are depicted in Fig. 4(a) and (b) respectively. A spatial multiplexing technique has been applied to the correlation filter (CGH) in order to achieve spatial separation of the mode power signals in the Fourier plane allowing simultaneous analysis of all the guided modes. Each diffraction pattern imaged on CCD_2 consists of 6 spatially separated intensity distributions (called correlation answers and denoted by white crosses in Fig. 4). The intensity signal recorded at each correlation answer, corresponding to selected pixels on CCD_2, is directly proportional to the power guided by the respective mode labeled ρ^2. In Fig. 4(a), the intensity measured at each correlation function is zero except for the LP_{01} mode, indicating a quasi-SM FUT beam. On the other hand, Fig. 4(b) shows a significantly different diffraction pattern where non-zero intensity is measured at several correlation answers, indicating the presence of multiple guided HOMs. In addition, phase channels (intentionally not indicated in Fig. 4), are also available on the CGH for each guided mode. As a result, the total vector-valued field emerging the FUT has been calculated and results are represented on top of Fig. 4(a) and (b) for the quasi-SM and the MM

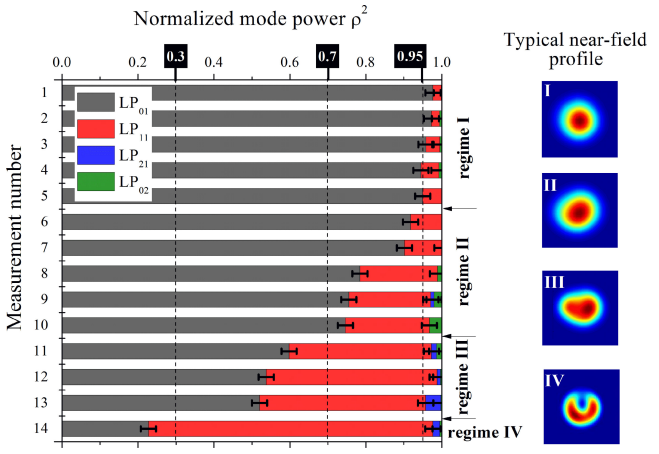

Fig. 5. CFT mode decomposition of 14 selected FUT beams. Measurements are sorted from low to high HOM content and each color represents a guided LP mode. The constant measurement error of $\pm 2\%$ is shown on the plot. Typical FUT beams are depicted on the right-hand for each modal regime.

beam respectively. In both cases, the reconstructed profile and the FUT near-field measured on CCD_1 show a good agreement.

Thus, the combined experiment benefits from the direct complementarity between S^2 imaging and CFT mode analysis techniques, enabling to achieve an advanced characterization of optical fibers with access to individual scalar and vector-valued field components.

V. Evaluation of Individual Mode Powers

It is well known that S^2 imaging mode analysis excels to measure extremely small HOM contents and the common method to calculate mode powers relies on strict assumptions [10], [15]. To date, S^2 imaging has been considered accurate when decomposing beams carrying one dominant mode. Recently, Nguyen *et al.* proposed a method to increase the accuracy of S^2 imaging when decomposing beams carrying more than two modes by identifying so-called spurious modes in the Fourier spectrum [38]. Most interestingly, Otto *et al.* [39] numerically demonstrated that S^2 imaging accuracy can be considerably improved employing general analytical mode evaluation algorithms. In this section, we experimentally investigate the accuracy S^2 analysis when employing different evaluation approaches.

A. Decomposition of a Wide Variety of Beams Using CFT

Fourteen different mode combinations have been excited in the FUT and decomposed using the combined experiment. For each FUT beam, the power of individual guided modes is evaluated with CFT. The intensity measured at the correlation answers (see Fig. 4) scales proportionally to the power $\rho^2(n)$ carried by the nth mode. After normalization, mode power results are presented in the bar diagram Fig. 5. It is important to note that both contributions from $LP_{11,e}$ and $LP_{11,o}$ ($LP_{21,e}$ and $LP_{21,o}$) measured in Fig. 4 are summed resulting in LP_{11} (respectively LP_{21}) in Fig. 5. Measured FUT beams are numbered from one to fourteen and are sorted from smaller to larger HOM content. Each LP mode is represented by a different color. For clarity purposes, four modal regimes, labeled from I to IV, are distinguished, corresponding to different mode mixtures. Regime I includes quasi-SM beams defined by $\rho^2(LP_{01}) \geq 95\%$. Regime II refers to beams carrying some HOM content but in which the fundamental mode dominates such that $0.95 \geq \rho^2(LP_{01}) \geq 0.7$. Regime III comprises MM beams where $0.7 \geq \rho^2(LP_{01}) \geq 0.3$ and finally, regime IV contains beams where the LP_{11} mode is dominantly excited (corresponding to measurement 14). Each regime is indicated in Fig. 5 and a typical FUT near-field profile is shown on the right hand side. One can clearly observe the beam distortion as the HOM content increases.

The accuracy of CFT mode evaluation mainly relies on the detector employed to record the diffraction pattern. In the present case, CCD_2 exhibits low quantum efficiency at 1064 nm wavelength and certain low modal amplitudes vanish in the background noise of the detector. Since the highest mode purity of the fundamental mode was measured around 98%, CFT mode evaluation error is fixed at $+/-2\%$ regardless of the modal regime. These error bars are indicated in Fig. 5. Thus, mode power evaluation from CFT can be considered as reliable across the wide range of FUT beams measured.

B. S^2 Imaging Evaluation Methods

The mode powers of all fourteen FUT beams reported in Fig. 5 have been evaluated using S^2 imaging measurements. To the best of our knowledge, this is the first time S^2 imaging analysis results of SM to MM beams can be directly compared to a second independent mode analysis technique. Two distinct analytical methods suggested in [39] have been applied to evaluate the mode powers from S^2 imaging measurement. Fig. 6(a)–(d) shows the normalized mode powers results for each of the fourteen measured FUT beams. Each plot corresponds to a modal regime defined in Fig. 5 with a scaled mode power axis. Guided modes are represented with different colors: LP_{01} in black, LP_{11} in red and LP_{21} in blue. The ρ^2 values previously evaluated from CFT (see Fig. 5) offer a direct comparison to S^2 evaluation and are represented using square markers in Fig. 6 and show the $+/-2\%$ measurement error.

The first mode power evaluation, called method 1 [39], is the general evaluation method employed in most S^2 imaging measurements to date (see list of applications in Section II-A). It relies on the strict assumption that most of the power is carried by one dominant mode. As a result, the value of $\rho^2(LP_{01})$ is approximately equal to the amplitude of the Fourier DC component (peak at zero DGD in Fig. 2) and the HOMs mode powers can be directly calculated. Results of method 1 are represented in Fig. 6(a)–(d) using hollow circle markers. A second evaluation method, called method 2 [39], is an analytical expression defined from the general expression of N-interfering modes (relation (4) and (5) in [39]) particularly suitable when the power is distributed among several HOMs. The evaluation results employing method 2 are represented using plain diamond markers in Fig. 6(a)–(d).

In Fig. 6(a), corresponding to regime I, the approximation of one dominant mode applies and evaluating $\rho^2(LP_{01})$ and $\rho^2(LP_{11})$ using method 1 and 2 (circle and diamond markers)

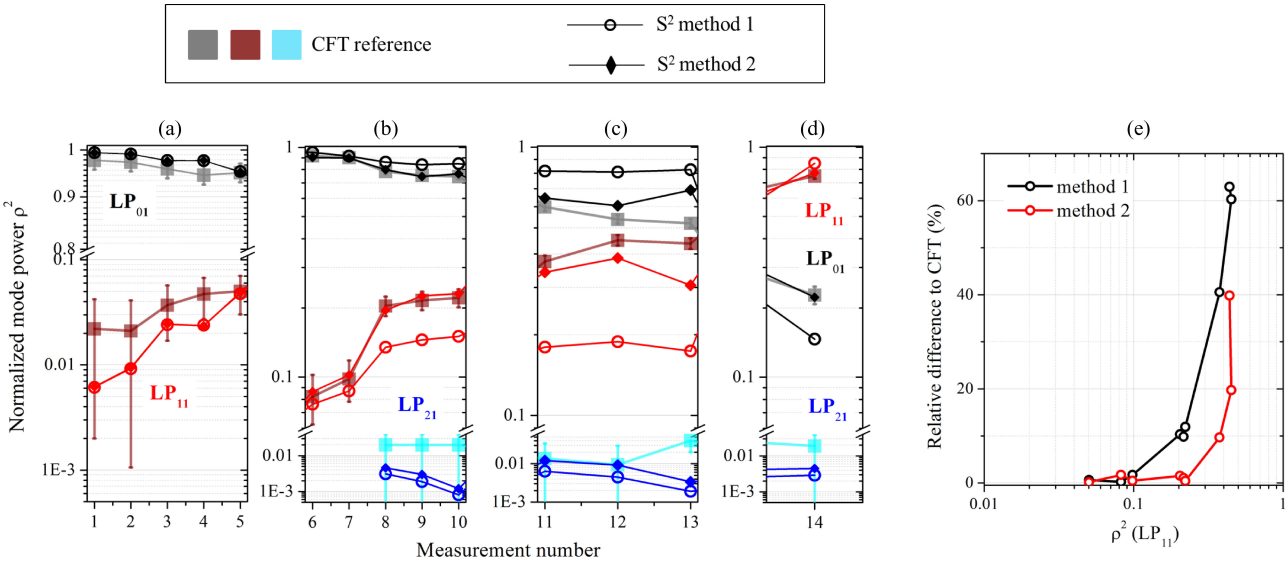

Fig. 6. (a)–(d) Modal decomposition of 14 FUT beams measured with the combined experiment. Normalized mode powers are evaluated from CFT (squares) and from S^2 imaging employing methods 1 (circle) and 2 (diamonds) [39] for individual guided modes. (e) Relative difference between evaluation methods 1 and 2 and CFT calculated for measurements 5 to 13 showing an increased S^2 imaging accuracy when using method 2.

perfectly overlaps. It is noteworthy that HOM powers as low as $\rho^2(\mathrm{LP}_{11}) \approx 0.006$ can be calculated from S^2 imaging measurements whereas CFT resolution is limited by the measurement error in this modal regime. This is also illustrated when evaluating $\rho^2(\mathrm{LP}_{21})$ (blue lines) in Fig. 6(b).

In regime II [see Fig. 6(b)], mode powers evaluated with methods 1 and 2 differ. However, $\rho^2(\mathrm{LP}_{01})$ and $\rho^2(\mathrm{LP}_{11})$ calculated with method 2 (diamonds) show a very good match with CFT results (squares). In this regime, the strict approximation of a dominant mode does not apply resulting in inaccurate S^2 imaging evaluation with method 1.

Reaching regime III [see Fig. 6(c)], $\rho^2(\mathrm{LP}_{01})$ and $\rho^2(\mathrm{LP}_{11})$ evaluated with method 2 differ from CFT results as the HOM mixtures increase (in particular for measurement 12 and 13). In this regime, mode identification from the Fourier spectrum becomes difficult due to the multiple mode mixings in addition to the distributed scattering occurring in this fiber.

Finally, regime IV [see Fig. 6(d)] is similar to regime II except that LP_{11} carries most of the power. Evaluation results of $\rho^2(\mathrm{LP}_{01})$ and $\rho^2(\mathrm{LP}_{11})$ using method 2 are in agreement with CFT results. In addition, S^2 imaging evaluation of low HOM content ($\rho^2(\mathrm{LP}_{21})$) provides an unmatched accuracy regardless of the method employed.

For completeness, it is important to mention that a third S^2 imaging evaluation method based on a general analytical mode reconstruction has been suggested in [39] when measuring three guide modes or more. However, in the present study, no inter-HOM interference peak could clearly be identified from the Fourier spectrum and this evaluation method couldn't be used.

Finally, the accuracy of S^2 imaging mode evaluation has been quantified. To do so, we consider the evaluation of the mode power $\rho^2(\mathrm{LP}_{11})$ for measurements 5 to 13. In this range ($\rho^2(\mathrm{LP}_{11}) \geq 0.04$), CFT provides a relatively accurate mode power evaluation that can be used as a reference. The relative difference between S^2 imaging evaluation methods 1 and 2 and CFT has been calculated using 1-$\rho^2(\mathrm{LP}_{11}(S^2))/\rho^2(\mathrm{LP}_{11}(\mathrm{CFT}))$. Results are plotted in Fig. 6(e) in black and red respectively. The x-axis scales with the reference $\rho^2(\mathrm{LP}_{11}(\mathrm{CFT}))$. Experimentally, we could determine the relative difference between method 1 and CFT to be less than a few for $\rho^2(\mathrm{LP}_{11}(\mathrm{CFT})) \leq 0.1$. For higher values of $\rho^2(\mathrm{LP}_{11}(\mathrm{CFT}))$ (measurement 8 to 13), the relative difference of method 1 to CFT considerably increases indicating that S^2 imaging mode evaluation is not accurate. In comparison, we experimentally demonstrate that employing method 2, the relative difference to CFT is less than a few percent up to $\rho^2(\mathrm{LP}_{11}(\mathrm{CFT})) \leq 0.3$ which considerably increases the modal detection limit of S^2 imaging. For larger mode mixing, S^2 imaging evaluation fails due to the complexity of the Fourier analysis.

VI. Conclusion

To conclude, a novel experimental tool for mode analysis is presented and combines, for the first time of our knowledge, two different and widely used mode analysis techniques. In addition to provide an advanced modal decomposition of optical fibers (with access to scalar and vector-valued fields), the combined experiment offers the unique capability to simultaneously decompose one beam using CFT and S^2 imaging. The direct comparison between mode powers evaluated from CFT analysis and S^2 imaging has led to experimentally confirm that S^2 imaging modal evaluation accuracy is considerably improved when employing a generalized analytical numerical routine (method 2 [39]).

To the best of our knowledge, we demonstrate, for the first time, that S^2 imaging can accurately decompose beams where the fundamental mode carries as low as 70% of the guided light. A complete summary of the expertise of each mode analysis technique is presented in Table I. The main differences between S^2 imaging and CFT are highlighted as well as the strengths

TABLE I
COMPARISON BETWEEN MODE ANALYSIS TECHNIQUES

	S^2 imaging	CFT
Relying on a prior knowledge of internal fiber parameters	No	Yes
Underlying mode analysis principle	Spatially and spectrally resolved multimode interference	Spatial correlation by means of a holographic filter
Necessary spectral bandwidth	- Broadband source (few tens of nm) [10] - Narrow line-width tunable laser source [25]	Narrow line-width source (< 1 nm)
Measurement + computation time	Few minutes to few hours (*)	0.03 s(**)
Real-time capability	No	Yes (depending on camera/detector system)
Detection and distinction between degenerated modes	No	Yes
Reconstruction of guided modes amplitude and phase profiles	Yes	No
Distinction between discrete and distributed mode scattering and unambiguous localization along the fiber length	Yes [15]	No (FUT is treated as a black box)
Mode power evaluation	Indirect (analytical method 1 or 2 [39])	Direct intensity measurement
Upper higher-order mode detection limit	Up to $\rho^2 \approx 0.3$ using method 2 [39]	$\rho^2 \approx 0.98$(**)
Lower higher-order mode detection limit	$\rho^2 \approx 0.006$(***)	$\rho^2 \approx 0.02$(**)
Limitations	- Complex mode identification when measuring MM beams - Tailored fiber length and source bandwidth	Measurement accuracy depends on number of detected modes

(*): Considerably reduced when using a tunable laser source.
(**): With the employed camera and wavelength.
(***): In this particular fiber under test (FUT).

and current limitations determined from the combined experiment results. Some challenges currently remain when evaluating highly MM beams (measurement 12 and 13) with S^2 imaging due to the complexity of the Fourier spectrum analysis. In this regime, CFT analysis provides unmatched mode decomposition capabilities.

REFERENCES

[1] C. Jauregui, J. Limpert, and A. Tünnermann, "High power fibre lasers," *Nat. Photon.*, vol. 7, pp. 861–867, 2013.

[2] D. J. Richardson, J. Nilsson, and W. Clarkson, "High power fiber lasers: Current status and future perspectives," *J. Opt. Soc. Amer. B*, vol. 27, no. 11, pp. B63–B92, 2010.

[3] F. Stutzki, F. Jansen, T. Eidam, A. Steinmetz, C. Jauregui, J. Limpert, and A. Tünnermann, "High average power large-pitch fiber amplifier with robust single-mode operation," *Opt. Lett.*, vol. 36, no. 5, pp. 689–691, 2011.

[4] F. Stutzki, F. Jansen, A. Liem, C. Jauregui, J. Limpert, and A. Tünnermann, "26 mJ, 130 W Q-switched fiber-laser system with near-diffraction-limited beam quality," *Opt. Lett.*, vol. 37, no. 6, pp. 1073–1075, 2012.

[5] Y. Kawahitoa, T. Terajimaa, H. Kimurab, T. Kurodaa, K. Nakataa, S. Katayamaa, and A. Inoueb, "High-power fiber laser welding and its application to metallic glass Zr55Al10Ni5Cu30," *Mat. Sci. Eng. B*, vol. 148, no. 1–3, pp. 105–109, 2008.

[6] P. Sprangle, A. Ting, J. Peñano, R. Fischer, and B. Hafizi, "Incoherent combining and atmospheric propagation of high-power fiber lasers for directed-energy applications," *IEEE J. Quantum Electron.*, vol. 45, no. 2, pp. 138–148, 2009.

[7] T. Bilici, S. Mutlu, H. Kalaycioqlu, A. Kurt, A. Sennaroqlu, and M. Gulsoy, "Development of a thulium (Tm:YAP) laser system for brain tissue ablation," *Las. Med. Sci.*, vol. 26, no. 5, pp. 699–706, 2011.

[8] C. Jauregui, T. Eidam, H.-J. Otto, F. Stutzki, F. Jansen, J. Limpert, and A. Tünnermann, "Temperature-induced index gratings and their impact on mode instabilities in high-power fiber laser systems," *Opt. Exp.*, vol. 20, no. 1, pp. 440–451, 2012.

[9] S. Wielandy, "Implication of higher-order mode content is large mode area fiber with good beam quality," *Opt. Exp.*, vol. 15, no. 23, pp. 15402–15409, 2007.

[10] J. W. Nicholson, A. D. Yablon, S. Ramachandran, and S. Ghalmi, "Spatially and spectrally resolved imaging of modal content in large-mode-area fibers," *Opt. Exp.*, vol. 16, no. 10, pp. 7233–7243, 2008.

[11] Y. Z. Ma, Y. Sych, G. Onishchukov, S. Ramachandran, U. Peschel, B. Schmauss, and G. Leuchs, "Fiber-modes and fiber anisotropy characterization using low-coherence interferometry," *Appl. Phys. B*, vol. 96, pp. 345–353, 2009.

[12] T. Kaiser, D. Flamm, S. Schröter, and M. Duparré, "Complete modal decomposition for optical fibers using CGH-based correlation filters," *Opt. Exp.*, vol. 17, no. 11, pp. 9347–9356, 2009.

[13] D. N. Schimpf, R. A. Barankov, and S. Ramachandran, "Cross-correlated (C2) imaging of fiber and waveguide modes," *Opt. Exp.*, vol. 19, no. 14, pp. 13008–13019, 2011.

[14] F. Stutzki, H.-J. Otto, F. Jansen, C. Gaida, C. Jauregui, J. Limpert, and A. Tünnermann, "High-speed modal decomposition of mode instabilities in high-power fiber lasers," *Opt. Lett.*, vol. 36, no. 23, pp. 4572–4574, 2011.

[15] J. W. Nicholson, A. D. Yablon, J. M. Fini, and M. D. Mermelstein, "Measuring the modal content of large-mode-area- fibers," *IEEE J. Sel. Topics Quantum Electron.*, vol. 15, no. 1, pp. 61–70, Jan. 2009.

[16] J. Bromage, J. M. Fini, C. Dorrer, and J. D. Zuegel, "Characterization and optimization of Yb-doped photonic-crystal fiber rod amplifier using spatially resolved spectral interferometry," *App. Opt.*, vol. 50, no. 14, pp. 2001–2007, 2011.

[17] F. Kong, K. Saitoh, D. Mcclane, T. Hawkins, P. Foy, G. Gu, and L. Dong, "Mode area scaling with all-solid photonic bandgap fibers," *Opt. Exp.*, vol. 20, no. 24, pp. 26363–26372, 2012.

[18] J. M. Fini, J. W. Nicholson, R. S. Windeler, E. M. Monberg, L. Meng, B. Mangan, A. DeSantolo, and F. V. DiMarcello, "Low-loss hollow-core fibers with improved single-modedness," *Opt. Exp.*, vol. 21, no. 5, pp. 6233–6242, 2013.

[19] J. Kerttula, V. Filippov, V. Ustimchik, Y. Chamorovskiy, and O. G. Okhotnikov, "Mode evolution in long tapered fibers with high tapering ratio," *Opt. Exp.*, vol. 20, no. 23, pp. 25461–25470, 2012.

[20] J. F. Bauters, M. L. Davenport, M. J. R. Heck, J. K. Doylend, A. Chen, A. W. Fang, and J. E. Bowers, "Silicon on ultra-low-loss waveguide photonic integration platform," *Opt. Exp.*, vol. 21, no. 1, pp. 544–555, 2013.

[21] J. W. Nicholson, L. Meng, J. M. Fini, R. S. Windeler, A. DeSantolo, E. Monberg, F. DiMarcello, Y. Dulashko, M. Hassan, and R. Ortiz, "Measuring higher-order modes in a low-loss, hollow-core, photonic-bandgap fiber," *Opt. Exp.*, vol. 20, no. 18, pp. 20494–20505, 2012.

[22] J. W. Nicholson, J. M. Fini, A. M. DeSantolo, X. Liu, K. Feder, P. S. Westbrook, V. R. Supradeepa, E. Monberg, F. DiMarcello, R. Ortiz, C. Headley, and D. J. DiGiovanni, "Scaling the effective area of higher-order-mode erbium-doped fiber amplifiers," *Opt. Exp.*, vol. 20, no. 22, pp. 24575–24584, 2012.

[23] P. Kadwani, C. Jollivet, R. A. Sims, A. Schülzgen, L. Shah, and M. Richardson, "Comparison of higher-order mode suppression and *Q*-switched laser performances in thulium-doped large mode area and photonic crystal fibers," *Opt. Exp.*, vol. 20, no. 22, pp. 24295–24303, 2012.

[24] G. Gu, F. Kong, T. W. Hawkins, P. Foy, K. Wei, B. Samson, and L. Dong, "Impact of fiber outer boundaries on leaky mode losses in leakage channel fibers," *Opt. Exp.*, vol. 21, no. 20, pp. 24039–24048, 2013.

[25] J. Jasapara and A. D. Yablon, "Spectrogram approach to S^2 fiber mode analysis to distinguish between dispersion and distributed scattering," *Opt. Lett.*, vol. 37, no. 18, pp. 3906–3908, 2012.
[26] M. A. Golub, A. M. Prokhorov, I. N. Sisakian, and V. A. Soifer, "Synthesis of spatial filters for investigation of the transverse mode composition of coherent radiation," *Sov. J. Quantum Electron.*, vol. 12, no. 9, pp. 1208–1209, 1982.
[27] W. H. Lee, "Sampled Fourier transform hologram generated by computer," *Appl. Opt.*, vol. 9, no. 3, pp. 639–643, 1970.
[28] D. Flamm, O. A. Schmidt, C. Schulze, J. Borchardt, T. Kaiser, S. Schröter, and M. Duparré, "Measuring the spatial polarization distribution of multimode beams emerging from passive step-index large-mode-area fibers," *Opt. Lett.*, vol. 35, no. 20, pp. 3429–3431, 2010.
[29] C. Schulze, O. A. Schmidt, D. Flamm, M. Duparré, and S. Schröter, "Modal analysis of beams emerging from a multi-core fiber using computer-generated holograms," *Proc. SPIE*, vol. 7914, 2011, doi: 10.1117/12.874732.
[30] D. Flamm, D. Naidoo, C. Schulze, A. Forbes, and M. Duparré, "Mode analysis with a spatial light modulator as a correlation filter," *Opt. Lett.*, vol. 37, no. 13, pp. 2478–2480, 2012.
[31] C. Schulze, A. Lorenz, D. Flamm, A. Hartung, S. Schröter, H. Bartelt, and M. Duparré, "Mode resolved bend loss in few-mode optical fibers," *Opt. Exp.*, vol. 21, no. 3, pp. 3170–3181, 2013.
[32] A. Dudley, I. A. Litvin, and A. Forbes, "Quantitative measurement of the orbital angular momentum density of light," *Appl. Opt.*, vol. 51, no. 7, pp. 823–833, 2012.
[33] D. Flamm, C. Schulze, R. Brüning, O. A. Schmidt, T. Kaiser, S. Schröter, and M. Duparré, "Fast M^2 measurement for fiber beams based on mode analysis," *Appl. Opt.*, vol. 51, no. 7, pp. 987–993, 2012.
[34] C. Schulze, D. Naidoo, D. Flamm, O. A. Schmidt, A. Forbes, and M. Duparré, "Wavefront reconstruction by modal decomposition," *Opt. Exp.*, vol. 20, no. 18, pp. 19714–19725, 2012.
[35] S. Shwartz, M. Golub, and S. Ruschin, "Diffractive optical elements for mode-division multiplexing of temporal signals with the aid of Laguerre–Gaussian modes," *Appl. Opt.*, vol. 52, no. 12, pp. 2659–2669, 2013.
[36] D. Flamm, C. Schulze, D. Naidoo, S. Schröter, A. Forbes, and M. Duparré, "All-digital tool for mode excitation and analysis in optical fibers," *IEEE J. Lightw. Tech.*, vol. 31, no. 7, pp. 1023–1032, Apr. 2013.
[37] D. Flamm, K.-C. Hou, P. Gelszinnis, C. Schulze, S. Schröter, and M. Duparré, "Modal characterization of fiber-to-fiber coupling processes," *Opt. Lett.*, vol. 38, no. 12, pp. 2128–2130, 2013.
[38] D. M. Nguyen, S. Blin, T. N. Nguyen, S. D. Le, L. Provino, M. Thual, and T. Chartier, "Modal decomposition technique for multimode fibers," *Appl. Opt.*, vol. 51, no. 4, pp. 450–456, 2012.
[39] H. J. Otto, F. Jansen, F. Stutzki, C. Jauregui, J. Limpert, and A. Tünnermann, "Improved modal reconstruction for spatially and spectrally resolved imaging," *IEEE J. Lightw. Tech.*, vol. 31, no. 8, pp. 1295–1299, Apr. 2013.

Authors' biography not available at the time of publication.